J|A|C|S
ARTICLES

Published on Web 04/20/2009

Preparation and Gas Adsorption Studies of Three Mesh-Adjustable Molecular Sieves with a Common Structure

Shengqian Ma,† Daofeng Sun, Daqiang Yuan, Xi-Sen Wang, and Hong-Cai Zhou*

Department of Chemistry, Texas A&M University, P.O. Box 30012, College Station, Texas 77842-3012

Received November 12, 2008; E-mail: zhou@mail.chem.tamu.edu

Abstract: Solvothermal reactions of a predesigned amphiphilic ligand, 4′-*tert*-butyl-biphenyl-3,5-dicarboxylate (BBPDC), with $Zn(NO_3)_2$, $Co(NO_3)_2$, and $Cu(NO_3)_2$ gave rise to three isostructural mesh-adjustable molecular sieves (MAMSs), MAMS-2, MAMS-3, and MAMS-4, respectively. The three new MAMSs all exhibit temperature-tuned molecular sieving effect. There exists a linear relationship between mesh size and temperature, $D = D_0 + \alpha T$ (D, mesh size at temperature T K; D_0, mesh size at 0 K; and α, constant). Constants D_0 and α are characteristics of a ligand in a certain structure, independent of the choice of metal. As a result, all of the three MAMSs based on the BBPDC ligand have a D_0 of 2.83 and an α of 0.0073.

Introduction

Molecular sieves are porous materials that can selectively adsorb molecules on the basis of their sizes. They have been widely used in shape/size selective catalysis and separation.[1] Conventionally, molecular sieves are made of inorganic zeolites. Due to the rigidity of the bonds in such materials, a molecular sieve is made with a fixed mesh size. This is beneficial when the mesh size precisely fits the separation needs. However, when the size difference of the two gases is very small, a molecular sieve with the precise mesh size is not always readily available. In such cases, mesh-adjustable molecular sieves (MAMSs) that can always meet the separation needs are highly desirable.

In order to make a MAMS, two factors—permanent porosity and flexibility of the pores—must be taken into account. Although a titanosilicate zeolite was reported to possess discrete mesh sizes based on the degree of dehydration of this material at various temperatures,[2] these two factors would seem irreconcilable for inorganic zeolites due to their robust frameworks.

As a new type of zeolitic analogues, porous metal−organic frameworks (MOFs)[3] have in the past decade become a burgeoning research field due to their potential applications in gas storage,[4] catalysis,[5] magnetism,[6] and gas separation.[7] In particular, the dynamic features[8] of porous MOFs have distinguished themselves from traditional inorganic zeolites and afforded the possibility to construct frameworks with flexible pores.[3b,8]

Scheme 1. (a) 5-*tert*-Butyl-1,3-benzenedicarboxylate (BBDC) and (b) 4′-*tert*-Butyl-biphenyl-3,5-dicarboxylate (BBPDC)

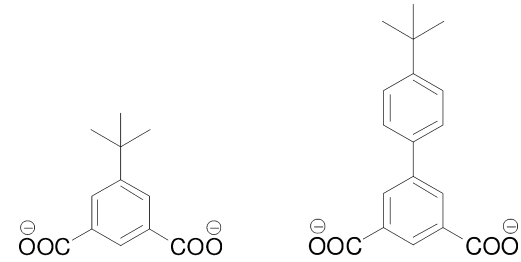

(a) (b)

Recently, we reported the first MOF-based mesh-adjustable molecular sieve, MAMS-1, built from the amphiphilic ligand 5-*tert*-butyl-1,3-benzenedicarboxylate (BBDC) (scheme 1a).[9] The mesh range of MAMS-1 falls between 2.9 and 5.0 Å. When the temperature is precisely controlled, any mesh size within this range can be accurately attained. In addition, a linear relationship between mesh size and temperature, $D = D_0 + \alpha T$ (eq 1: D, mesh size at temperature T K; D_0, mesh size at 0 K;

† Current address: Chemical Sciences and Engineering Division, Argonne National Laboratory, 9700 S. Cass Ave., Argonne, IL 60439.

(1) Davis, M. E. *Nature (London)* **2002**, *417*, 813.
(2) Kuznicki, S. M.; Bell, V. A.; Nair, S.; Hillhouse, H. W.; Jacubinas, R. M.; Braunbarth, C. M.; Toby, B. H.; Tsapatsis, M. *Nature (London)* **2001**, *412*, 720.
(3) (a) Eddaoudi, M.; Moler, D. B.; Li, H.; Chen, B.; Reineke, T. M.; O'Keeffe, M.; Yaghi, O. M. *Acc. Chem. Res.* **2001**, *34*, 319. (b) Kitagawa, S.; Kitaura, R.; Noro, S.-i. *Angew. Chem., Int. Ed.* **2004**, *43*, 2334. (c) Férey, G. *Chem. Soc. Rev.* **2008**, *37*, 191. (d) Suh, M. P.; Cheon, Y. E.; Lee, E. Y. *Coord. Chem. Rev.* **2008**, *252*, 1007.
(4) (a) Chen, B.; Ockwig, N. W.; Millward, A. R.; Contrereas, D. S.; Yaghi, O. M. *Angew. Chem., Int. Ed.* **2005**, *44*, 4745. (b) Sun, D.; Ma, S.; Ke, Y.; Collins, D. J.; Zhou, H.-C. *J. Am. Chem. Soc.* **2006**, *128*, 3896. (c) Ma, S.; Zhou, H.-C. *J. Am. Chem. Soc.* **2006**, *128*, 11734. (d) Dinca, M.; Dailly, A.; Liu, Y.; Brown, C. M.; Neumann, D. A.; Long, J. R. *J. Am. Chem. Soc.* **2006**, *128*, 16876. (e) Wang, X.-S.; Ma, S.; Sun, D.; Parkin, S.; Zhou, H.-C. *J. Am. Chem. Soc.* **2006**, *128*, 16474. (f) Ma, S.; Sun, D.; Ambrogio, M. W.; Fillinger, J. A.; Parkin, S.; Zhou, H.-C. *J. Am. Chem. Soc.* **2007**, *129*, 1858. (g) Collins, D. J.; Zhou, H.-C. *J. Mater. Chem.* **2007**, *17*, 3154. (h) Ma, S.; Sun, D.; Simmons, J. M.; Collier, C. D.; Yuan, D.; Zhou, H.-C. *J. Am. Chem. Soc.* **2008**, *130*, 1012. (i) Wang, X.-S.; Ma, S.; Rauch, K.; Simmons, J. M.; Yuan, D.; Wang, X.; Yildirim, T.; Cole, W. C.; López, J. J.; de Meijere, A.; Zhou, H.-C. *Chem. Mater.* **2008**, *20*, 3145. (j) Wang, X.-S.; Ma, S.; Forster, P. M.; Yuan, D.; Eckert, J.; López, J. J.; Murphy, B. J.; Parise, J. B.; Zhou, H.-C. *Angew Chem. Int. Ed.* **2008**, *47*, 7263. (k) Ma, S.; Eckert, J.; Forster, P.; Yoon, J.; Hwang, Y. K.; Chang, J.-S.; Collier, C. D.; Parise, J. B.; Zhou, H.-C. *J. Am. Chem. Soc.* **2008**, *130*, 15896.

and α, constant), was discovered. Moreover, mechanistic studies of the molecular gating effect of MAMS-1, which is controlled by the *tert*-butyl groups of the BBDC ligand, suggest that D_0 and α can be tuned by ligand design. This implies the possibility of a MAMS that will be versatile in gas separation even at ambient temperatures. In order to test the feasibility of the hypothesis and explore new MAMSs for gas separation, herein we present a new ligand 4′-*tert*-butyl-biphenyl-3,5-dicarboxylate (BBPDC) (Scheme 1b), which has one more phenyl ring than BBDC. As expected, solvothermal reactions of BBPDC with $Zn(NO_3)_2$, $Co(NO_3)_2$, and $Cu(NO_3)_2$ give rise to MAMS-2, MAMS-3, MAMS-4, respectively. The three new MAMSs are isostructural but quite different from the structure of MAMS-1, and all display a temperature-induced molecular sieving effect similar to that observed in MAMS-1 but with different D_0 and α values for eq 1. This also allows the assessment of the effect of the choice of metal (Zn, Co, or Cu) on the slope (α) and inception (D_0) of the linear relationship between mesh size and temperature; there is none. Thus, the most likely means to tune D_0 and α values in eq 1 is through ligand design.

Experimental Section

General Information. Commercially available reagents were used as received without further purification. Elemental analyses (C, H, and N) were obtained from Canadian Microanalytical Service Ltd. Thermal gravimetric analysis (TGA) was performed under N_2 on a PerkinElmer TGA 7 and a Beckman Coulter SA3100 surface area analyzer was utilized for the gas adsorption measurements. NMR data were collected on a Bruker 300 MHz spectrometer.

Synthesis of 4′-*tert*-Butyl-biphenyl-3,5-dicarboxylic Acid (H_2BBPDC). To a 500 mL Schlenk flask, dimethyl-5-bromo-isophtalate (2 g, 0.015 mol), 4-*tert*-butyl-phenyl boronic acid (4 g, 0.015 mol), CsF (2.3 g), and $Pd(PPh_3)_4$ (0.2 g) were added. The flask was connected to a Schlenk line while 300 mL of 1,2-dimethoxyethane was degassed and added through a cannula. The flask was equipped with a water condenser and refluxed under nitrogen for 48 h. The reaction mixture was dried, H_2O (100 mL) was added, and the solution was extracted with $CHCl_3$. The organic phase was dried with $MgSO_4$. After solvent removal, the crude product was purified by column chromatography (silica, $CHCl_3$) to give the pure product 4′-*tert*-butyl-biphenyl-3,5-dicarboxylate methyl ester (^{1}H NMR ($CDCl_3$): 1.4 (s, 9H), 3.9 (s, 3H), 7.3 (d, 2H), 7.5 (d, 2H), 8.4 (s, 2H), 8.6 (s, 1H)). 4′-*tert*-Butyl-biphenyl-3,5-dicarboxylate methyl ester was dissolved in a 100 mL mixture of THF and MeOH (v/v = 1:1), to which 20 mL of 2 N NaOH aqueous solution was added. The mixture was stirred at room temperature overnight. The organic phase was removed. The aqueous phase was acidified with diluted hydrochloric acid to give a white precipitate, which was filtered and washed with water several times to give H_2BBPDC (^{1}H NMR (DMSO): 1.4 (s, 9H), 7.5 (d, 2H), 7.6 (d, 2H), 8.3 (s, 2H), 8.4 (s, 1H)).

Synthesis of MAMS-2. A mixture of 20 mg of $Zn(NO_3)_2 \cdot 6H_2O$ and 10 mg of H_2BBPDC in 1.5 mL of dimethylformamide (DMF) solvent was sealed in a Pyrex glass tube (i.d. 8 mm/o.d. 10 mm) and heated to 120 °C at a rate of 1 °C/min. After staying at 120 °C for 24 h, it was cooled to 35 °C at a rate of 0.1 °C/min. The resulting colorless crystals were washed with DMF twice to give pure MAMS-2 ($Zn_2(H_2O)_2(BBPDC)_2 \cdot 3DMF$, yield = 85% based on H_3BBPDC). The reaction was amplified to gram quantity using multiple tubes. Anal. Calcd for MAMS-2: C 55.22%, H 5.87%, N 4.29%; found: C 55.65%, H 5.39%, N 3.98%.

Synthesis of MAMS-3. A mixture of 20 mg of $Co(NO_3)_2 \cdot 6H_2O$ and 10 mg of H_2BBPDC in 1.5 mL of dimethylacetamide (DMA) solvent was sealed in a Pyrex glass tube (i.d. 8 mm/o.d. 10 mm) and heated to 120 °C at a rate of 1 °C/min. After staying at 120 °C for 24 h, it was cooled to 35 °C at a rate of 0.1 °C/min. The resulting violet crystals were washed with DMA twice to give pure MAMS-3 ($Co_2(H_2O)_2(BBPDC)_2 \cdot 3DMA$, yield = 80% based on BBPDC ligand). The reaction was amplified to gram quantity using multiple tubes. Anal. Calcd for MAMS-3: C 57.20%, H 6.30%, N 4.17%; found: C 58.85%, H 6.16%, N 4.15%.

Synthesis of MAMS-4. A mixture of 20 mg of $Cu(NO_3)_2 \cdot 2.5H_2O$ and 10 mg of BBPDC ligand in 1.5 mL of DMF solvent with 3 drops of HBF_4 (50% aqueous solution) added was sealed in a Pyrex glass tube (i.d. 8 mm/o.d. 10 mm) and heated to 75 °C at a rate of 0.1 °C/min. After staying at 75 °C for 24 h, it was cooled to 35 °C at a rate of 0.1 °C/min. The resulting turquoise crystals were washed with DMA twice to give pure MAMS-4 ($Cu_2(H_2O)_2(BBPDC)_2 \cdot 3DMF$ yield = 80% based on BBPDC ligand). The reaction was amplified to gram quantity using multiple tubes. Anal. Calcd for MAMS-2: C 55.43%, H 5.89%, N 4.31%; found: C 55.13%, H 5.54%, N 4.58%.

Single-Crystal X-ray Crystallography. Single crystal X-ray data were collected on a Bruker Smart Apex diffractometer equipped with an Oxford Cryostream low-temperature device and a fine-focus sealed-tube X-ray source (Mo Kα radiation, λ = 0.71073 Å, graphite monochromated) operating at 45 kV and 35 mA. Frames were collected with 0.3° intervals in φ and ω for 30 s/frame such that a hemisphere of data was collected. Raw data collection and refinement were done using SMART. Data reduction was performed using SAINT+ and corrected for Lorentz and polarization effects. Adsorption corrections were applied using the SADABS routine.[10] The structure was solved by direct methods and refined by full-matrix least-squares on F^2 with anisotropic displacement using SHELX-97.[11] Non-hydrogen atoms were refined with anisotropic displacement parameters during the final cycles. Hydrogen atoms on carbon were calculated in ideal positions with isotropic displacement parameters set to $1.2U_{eq}$ of the attached atom.

(5) (a) Seo, J. S.; Whang, D.; Lee, H.; Jun, S. I.; Oh, J.; Jeon, Y. J.; Kim, K. *Nature (London)* **2000**, *404*, 982. (b) Hu, A.; Ngo, H. L.; Lin, W. *J. Am. Chem. Soc.* **2003**, *125*, 11490. (c) Zou, R.; Sakurai, H.; Xu, Q. *Angew. Chem., Int. Ed.* **2006**, *45*, 2542.

(6) (a) Halder, G. J.; Kepert, C. J.; Moubaraki, B.; Murray, K. S.; Cashion, J. D. *Science* **2002**, *298*, 1762. (b) Janiak, C. *J. Chem. Soc., Dalton Trans.* **2003**, 2781. (c) Zheng, Y.-Z.; Tong, M.-L.; Zhang, W.-X.; Chen, X.-M. *Angew. Chem., Int. Ed.* **2006**, *45*, 6310. (d) Yu, C.; Ma, S.; Pechan, M. J.; Zhou, H.-C. *J. Appl. Phys.* **2007**, *101*, 09E108.

(7) (a) Matsuda, R.; Kitaura, R.; Kitagawa, S.; Kubota, Y.; Belosludov, R. V.; Kobayashi, T. C.; Sakamoto, H.; Chiba, T.; Takata, M.; Kawazoe, Y.; Mita, Y. *Nature (London)* **2005**, *436*, 238. (b) Dinca, M.; Long, J. R. *J. Am. Chem. Soc.* **2005**, *127*, 9376. (c) Dybtsev, D. N.; Chun, H.; Yoon, S. H.; Kim, D.; Kim, K. *J. Am. Chem. Soc.* **2004**, *126*, 32. (d) Humphrey, S. M.; Chang, J.-S.; Jhung, S. H.; Yoon, J. W.; Wood, P. T. *Angew. Chem., Int. Ed.* **2006**, *46*, 272. (e) Chen, B.; Liang, C.; Yang, J.; Contreras, D. S.; Clancy, Y. L.; Lobkovsky, E. B.; Yaghi, O. M.; Dai, S. *Angew. Chem., Int. Ed.* **2006**, *45*, 1390. (f) Chen, B.; Ma, S.; Zapata, F.; Fronczek, F. R.; Lobkovsky, E. B.; Zhou, H.-C. *Inorg. Chem.* **2007**, *46*, 1233. (g) Ma, S.; Wang, X.-S.; Manis, E. S.; Collier, C. D.; Zhou, H.-C. *Inorg. Chem.* **2007**, *46*, 3432. (h) Ma, S.; Wang, X.-S.; Collier, C. D.; Manis, E. S.; Zhou, H.-C. *Inorg. Chem.* **2007**, *46*, 8499. (i) Chen, B.; Ma, S.; Hurtado, E. J.; Lobkovsky, E. B.; Zhou, H.-C. *Inorg. Chem.* **2007**, *46*, 8490. (j) Barcia, P. S.; Zapata, F.; Silva, J. A. C.; Rodrigues, A. E.; Chen, B. *J. Phys. Chem. B* **2007**, *111*, 6101–6103. (k) Bastin, L.; Barcia, P. S.; Hurtado, E. J. J.; Silva, A. C.; Rodrigues, A. E.; Chen, B. *J. Phys. Chem. C* **2008**, *112*, 1575–1181. (m) Ma, S.; Wang, X.-S.; Yuan, D.; Zhou, H.-C. *Angew. Chem., Int. Ed.* **2008**, *47*, 4130. (n) Li, K. H.; Olsan, D. H.; Lee, J. Y.; Bi, W. H.; Wu, K.; Yuen, T.; Xu, Q.; Li, J. *Adv. Funct. Mater.* **2008**, *18*, 2205. (o) Ma, S.; Yuan, D.; Wang, X.-S.; Zhou, H.-C. *Inorg. Chem.* **2009**, *48*, 2072.

(8) (a) Uemura, K.; Matsuda, R.; Kitagawa, S. *J. Solid State Chem.* **2005**, *178*, 2420. (b) Bradshaw, D.; Claridge, J. B.; Cussen, E. J.; Prior, T. J.; Rosseinsky, M. J. *Acc. Chem. Res.* **2005**, *38*, 273. (c) Kitagawa, S.; Kazuhiro, U. *Chem. Soc. Rev.* **2005**, *34*, 109.

(9) Ma, S.; Sun, D.; Wang, X.-S.; Zhou, H.-C. *Angew. Chem., Int. Ed.* **2007**, *46*, 2458.

(10) *SAINT+, version 6.22*; Bruker Analytical X-Ray Systems, Inc.: Madison, WI, 2001.

(11) Sheldrick, G. M. *SHELX-97*; Bruker Analytical X-Ray Systems, Inc.: Madison, WI, 1997.

In all cases solvent molecules were highly disordered, and attempts to locate and refine the solvent peaks were unsuccessful; contributions to scattering due to these solvent molecules were removed using the SQUEEZE routine of PLATON and refined further using the data generated.[12]

Gas Adsorption Measurements. Gas adsorption measurements were performed using a Beckman Coulter SA 3100 surface area and pore size analyzer. The samples were held under a dynamic vacuum ($<10^{-3}$ torr) at 300 °C for MAMS-2 and MAMS-3, or 170 °C for MAMS-4, for 5 h to remove the free guest solvent molecules (DMF or DMA) and coordinated aqua ligands. Before the measurement, the sample was evacuated again by using the "outgas" function of the surface area analyzer for 1 h at 300 °C for MAMS-2 and MAMS-3 or 170 °C for MAMS-4. A sample of about 100.0 mg was used for N_2 (99.999%) adsorption measurement and was maintained at 77 K with liquid nitrogen. In the hydrogen storage measurement, high purity hydrogen (99.9995%) and a 100.0 mg sample were used. The regulator and pipe were flushed with hydrogen before they were connected to the analyzer. The internal lines of the instrument were flushed three times by utilizing the "flushing lines" function of the program to ensure the purity of H_2. The measurement was maintained at 77 K with liquid nitrogen. Similar to the procedures used for H_2 measurement at 77 K, highly pure O_2 (99.99%), CO (99.99%), CH_4 (99.997%), C_2H_4 (99.5%), C_3H_6 (99.5%), *iso*-C_4H_{10} (99.5%), SF_6 (99.8%), and CO_2 (99.99%) were used for their respective gas adsorption measurements. All the gases used for the measurements were purchased from Linde Gas LLC (Cincinnati, OH). The temperatures at 87, 113, 143, 195, and 231 K were maintained with a liquid argon bath, isopentane−liquid nitrogen bath, *n*-pentane−liquid nitrogen bath, acetone−dry ice bath, and acetonitrile−dry ice bath, respectively.[13,14] To prevent condensation of CO and O_2 at 77 K, the pressure ranges were below 448 and 156 torr, respectively; to prevent condensation of O_2 at 87 K, the pressure range was below 466 torr; to prevent condensation of C_2H_4 at 143 K, the pressure range was below 120 torr; to prevent condensation of C_3H_6 at 195 K, the pressure range was below 110 torr; to prevent condensation of *iso*-C_4H_{10} at 231 K, the pressure range was below 210 torr. For all adsorption isotherms, P_0 represents a relative standard (pressure of the saturation tube of the Beckman Coulter SA 3100 surface area during the measurement): at 77 K, P_0 was 757 torr for H_2 and N_2, 441 torr for CO, and 151 torr for O_2; at 87 K, P_0 was 757 torr for CO and N_2 and 465 torr for O_2; at 113 K, P_0 was 757 torr for CO, CH_4, and N_2; at 143 K, P_0 was 757 torr for CH_4 and 118 torr for C_2H_4; at 195 K, P_0 was 757 torr for C_2H_4 and CO_2 and 108 torr for C_3H_6; at 241 K, P_0 was 757 torr for C_3H_6 and 205 torr for *iso*-C_4H_{10}; at 295 K, P_0 was 757 torr for *iso*-C_4H_{10} and SF_6.

Results and Discussion

Crystal Structure Description. Single-crystal X-ray studies reveal that the three new MAMSs are isostructual, and all of them crystallize in the space group $P\bar{3}c1$(Table 1). They adopt the well-known $M_2(COO)_4$ paddlewheel as their secondary building unit (SBU), where two aqua axial ligands can be removed at high activation temperature. This type of dimetal paddlewheel SBUs happens to be very common for copper MOFs[4a,c,h,i] and has also been frequently reported for zinc MOFs.[4f,7e,15] However, as for cobalt, MAMS-3 represents one of the very few instances of MOFs possessing the dicobalt paddlewheel SBU.[6c,16] Selected interatomic distances are listed in Table 2. The M···M distance varies from 2.647 for Cu to 2.951 Å for Zn. For all of the three MAMSs, the longer the M···M distance, the shorter the M−aqua distance. The trend of the interatomic distances seems to suggest that the stronger the M···M interaction (if any), the weaker the M−aqua bonding.

Table 1. Crystal Data[a] and Structure Refinement of MAMS-2, MAMS-3, and MAMS-4

	MAMS-2 (Zn)	MAMS-3 (Co)	MAMS-4 (Cu)
formula	$C_{18}H_{18}ZnO_5$	$C_{18}H_{18}CoO_5$	$C_{18}H_{18}CuO_5$
fw	379.69	373.25	377.86
crystal system	trigonal	trigonal	trigonal
space group	$P\bar{3}c1$	$P\bar{3}c1$	$P\bar{3}c1$
crystal size (mm^3)	0.16 × 0.12 × 0.10	0.18 × 0.15 × 0.10	0.15 × 0.13 × 0.10
a, Å	18.6069(6)	18.9328(1)	18.4472(4)
b, Å	18.6069(6)	18.9328(1)	18.4472(4)
c, Å	22.6226(1)	22.307(3)	22.5760(1)
α, deg	90.00	90.00	90.00
β, deg	90.00	90.00	90.00
γ, deg	120.00	120.00	120.00
V, Å^3	6783.0(5)	6924.7(1)	6653.3(4)
Z	12	12	12
d_{calcd}, g/cm	1.115	1.074	1.132
GOF	1.06	1.459	1.093
R1, wR2[b]	0.0746, 0.2043	0.0665, 0.203	0.0731, 0.2152

[a] Obtained with graphite-monochromated Mo Kα (λ = 0.71073 Å) radiation. [b] $R1 = \Sigma||F_o| - |F_c||/\Sigma|F_o|$ and $wR2 = \{[\Sigma w(F_o^2 - F_c^2)^2]/[\Sigma w(F_o^2)^2]\}^{1/2}$.

Table 2. Selected Bonding Distances in MAMS-2, MAMS-3, and MAMS-4

	MAMS-2 (Zn)	MAMS-3 (Co)	MAMS-4 (Cu)
M···M distances (Å)	2.951	2.876	2.647
M−aqua bonding distances (Å)	1.869	1.978	2.016

Each paddlewheel SBU connects four BBPDC ligands, while every BBPDC ligand connects two paddlewheel SBUs expanding into a 2-D layer with the hydrophilic paddlewheel SBUs sandwiched by two hydrophobic BBPDC layers (Figure 1). In each layer, every three paddlewheel SBUs are connected by three BBPDC ligands to form the triangular hydrophilic holes with the *tert*-butyl groups of every three BBPDC ligands pointing up and down alternately. Every six paddlewheel SBUs connect six BBPDC ligands, three of which point down and three of which point up, to form a hydrophobic cage with a volume of 1360 Å^3 for MAMS-2, 1386 Å^3 for MAMS-3, and 1341 Å^3 for MAMS-4. Every hydrophobic cage with S_6 symmetry is encircled by six hydrophilic holes with C_3 symmetry, and every hydrophilic hole is surrounded by three hydrophobic cages (Figure 2). In each hydrophobic cage, there are six vertical slits with the narrowest opening size of 9.71 Å

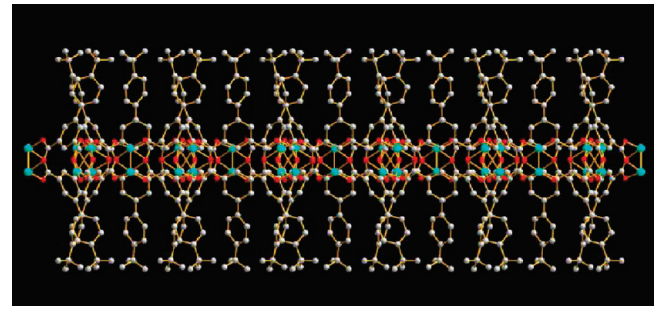

Figure 1. Structure of a 2-D sandwich layer.

(12) Spek, A. L. *J. Appl. Crystallogr.* **2003**, *36*, 7.
(13) Rondeau, R. E. *J. Chem. Eng. Data* **1966**, *11*, 124.
(14) Phipps, A. M.; Hume, D. N. *J. Chem. Educ.* **1968**, *45*, 664.
(15) (a) Dybtsev, D. N.; Chun, H.; Kim, K. *Angew. Chem., Int. Ed.* **2004**, *43*, 5033. (b) Chun, H.; Dybtsev, D. N.; Kim, H.; Kim, K. *Chem.—Eur. J.* **2005**, *11*, 3521. (c) Ma, B.-Q.; Mulfort, K. L.; Hupp, J. T. *Inorg. Chem.* **2005**, *44*, 4912.

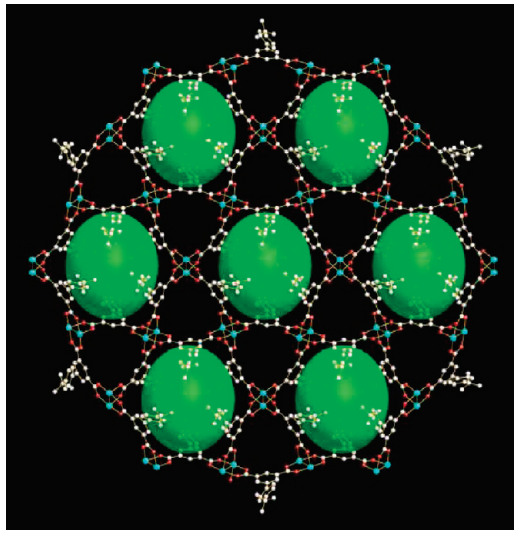

Figure 2. Hydrophilic holes (with C_3 symmetry) and hydrophobic cages (green spheres, with S_6 symmetry) in a sandwiched layer.

(atom-to-atom distance; ~6.6 Å when considering van der Waals radii[17]) for MAMS-2, 9.87 Å (atom-to-atom distance; ~6.8 Å when considering van der Waals radii[17]) for MAMS-3, and 9.60 Å (atom-to-atom distance; ~6.5 Å when considering van der Waals radii[17]) for MAMS-4 (Figure 3a).

Every layer interacts with adjacent layers through van der Waals interaction among *tert*-butyl groups between the adjacent layers (Figure 4) to form a graphitic structure. The triangular hydrophilic holes of each layer pack along *c* direction to form 1-D triangular hydrophilic channels with edge length of 7.82 Å for MAMS-2, 8.07 Å for MAMS-3, and 7.90 Å for MAMS-4 (metal atom-to-metal atom distances:~4.9 Å for MAMS-2, ~4.8 Å for MAMS-3, and ~4.9 Å for MAMS-4 when considering van der Waals radii[17]) after removal of the aqua ligands. The hydrophobic cages of each layer pack along *c* direction with the *tert*-butyl groups from the adjacent layers inserting into the vertical slits of the hydrophobic cages (Figure 3b). Viewed from the *c* direction, it can be inferred that the hydrophobic cages should be the main storage space for gas molecules, while the hydrophilic channels should act as passages to allow gas molecules to enter the cages through the space between the adjacent *tert*-butyl groups. These groups may serve as gates at the intersections of the hydrophilic channels and hydrophobic cages (Figure 5).

Thermal Gravimetric Analysis (TGA). As shown in Figure 6, the first 24.6% (cald, 26.0) weight loss of MAMS-2 from about 300 to 420 °C corresponds to the loss of three unbound DMF guest molecules and two coordinated aqua ligands. Decomposition of the BBPDC ligands starts from around 430 °C and ends at 650 °C with an overall weight loss of 56.4% (cald, 57.2%). As for MAMS-3, the loss of three unbound DMA guest molecules and two coordinated aqua ligands also starts from around 300 °C and ends at about 420 °C (cald, 29.5%; found, 28.0%), which is followed by the decomposition of the BBPDC ligands with an overall weight loss of 55.0% (cald, 55.6%). Finally for MAMS-4, the loss of three unbound DMF guest molecules and two coordinated aqua ligands starts from about 150 °C and ends at about 350 °C (cald, 29.5%; found, 28.0%), which is closely followed by the decomposition of the BBPDC ligands with the weight loss of 54.0% (cald, 57.5%) ending at around 430 °C. The thermal stability of MAMS-4 is comparable to that of other dicopper-paddlewheel-based MOFs,[4a,b] but less than that of MAMS-2 or MAMS-3. So far we do not have a satisfying explanation for the added thermal stability of MAMS-2 and MAMS-3 because paddlewheel structures of Zn and Co are far less common than those of Cu.

Gas Adsorption Studies. In order to investigate the temperature-induced molecular sieving effect of MAMS-2, the freshly isolated sample, which is not active for adsorption (Figure S1), was activated at 300 °C under a dynamic vacuum to remove the DMF guest molecules and coordinated aqua ligands. Subsequently, gas adsorption measurements were carried out at a variety of temperatures. As shown in Figure 7a, MAMS-2 exhibits highly selective adsorption of H_2 over CO, N_2, or O_2 (Figure 7a) at 77 K. Such selectivity in MOFs has previously been reported in several cases[7c,d,h] and was also observed in MAMS-1.[9] It is unlikely that this can be attributed to the size of the hydrophilic channels, which are around 4.9 Å (considering van der Waals radii) and are large enough to accommodate O_2, N_2, or CO molecules (kinetic diameters are 3.46, 3.64, and 3.76 Å for O_2, N_2, and CO, respectively).[18] This implies that the molecular sieving effect has a different origin.

The crystal structure of MAMS-2 shows that a hydrophobic cage is accessible only through its hydrophobic/hydrophilic interface, where the *tert*-butyl groups of BBPDC ligands serve as gates based on van der Waals attraction (Figure 3b). When such gates are open, the gas molecules in the hydrophilic channels are allowed to enter the hydrophobic cages.

Presumably, the molecular sieving effect comes from the *tert*-butyl groups. In view of the kinetic diameters of 2.89 Å for H_2, 3.46 Å for O_2, 3.64 Å for N_2, and 3.76 Å for CO,[18] it can be inferred that the gate opening of MAMS-2 is around 3.0−3.4 Å. At 77 K, MAMS-2 excludes CO, N_2, and O_2 but allows H_2 to enter the hydrophobic cages.

Therefore, the gates should open wider at higher temperatures because of the reduced van der Waals interaction among the *tert*-butyl groups, thus allowing larger molecules to pass the gate.

When the temperature is raised to liquid argon temperature (87 K, Figure 7b), gas adsorption studies reveal that only a small amount of CO or N_2 is adsorbed by MAMS-2. However, MAMS-2 can take up significant amounts of O_2. The adsorption isotherm of O_2 shows type-I behavior. Dioxygen (3.46 Å) can be selectively adsorbed from a mixture with N_2 (3.64 Å) and CO (3.76 Å), which implies that at 87 K the gate opens to around 3.5 Å. When the temperature is increased to 113 K, MAMS-2 can take up a moderate amount of N_2 but relatively low quantities of CO and CH_4 (3.8 Å) (Figure 7c), consistent with the suggestion that the gating effect is due to *tert*-butyl groups of BBPDC ligands, and the gate opens wider under increased temperatures. This also implies that at 113 K, the gate opens to about 3.7 Å, wide enough to allow N_2 (3.64 Å) to pass, but molecules with larger kinetic diameters such as CO (3.76 Å) and CH_4 (3.8 Å) will stay in the hydrophilic channels. The resolution for size discrimination is now 0.12 Å. In fact, it can be inferred from all the adsorption data obtained thus far

(16) (a) Choi, E.-Y.; Park, K.; Yang, C.-M.; Kim, H.; Son, J.-H.; Lee, S. W.; Lee, Y. H.; Min, D.; Kwon, Y.-U. *Chem.—Eur. J.* **2004**, *10*, 5535. (b) Chen, B.; Ma, S.; Hurtado, E. J.; Lobkovsky, E. B.; Liang, C.; Zhu, H.; Dai, S. *Inorg. Chem.* **2007**, *46*, 8705.
(17) Bondi, A. *J. Phys. Chem.* **1964**, *68*, 441.
(18) Beck, D. W. *Zeolite Molecular Sieves*; Wiley and Sons: New York, 1974.

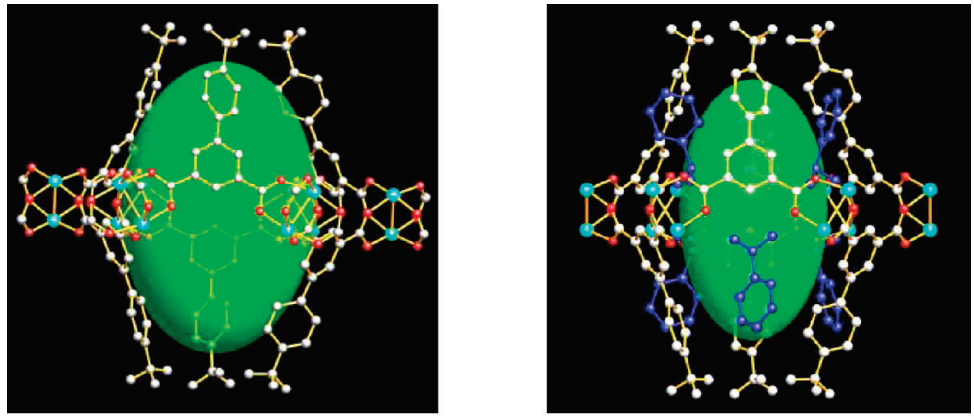

Figure 3. (a) Hydrophobic cage with six open vertical slits. (b) A hydrophobic cage with six *tert*-butyl groups (shown in blue) of BBPDC ligands from the adjacent layers inserting into the open slits by packing.

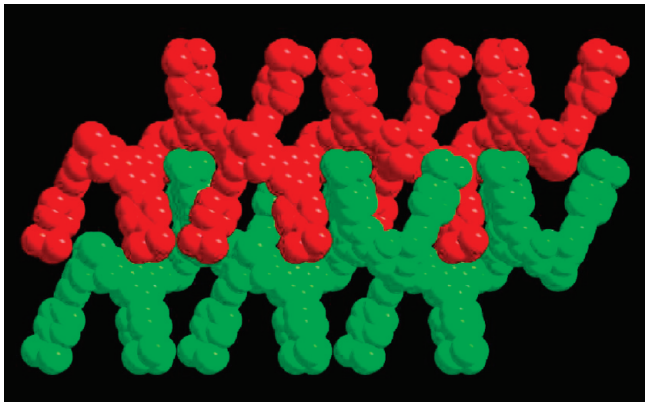

Figure 4. Two adjacent layers interact with each other through van der Waals interaction.

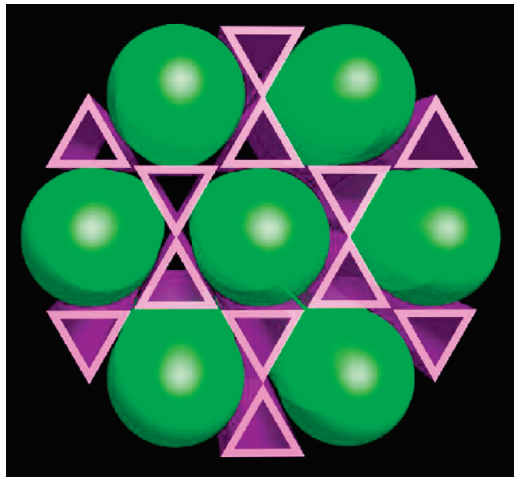

Figure 5. Hydrophilic channels and hydrophobic cages viewing along the *c* direction.

that if temperatures can be tuned continuously and precisely, any two molecules with a size difference can be separated by MAMS-2, as seen in MAMS-1.

With these considerations in mind, we decided to explore the possibility of using MAMS-2 in separations important to the petroleum refinery and petrochemical industry. Not surprisingly, MAMS-2 can distinguish methane from ethylene at 143 K, ethylene from propylene at 195 K, and propylene from isobutane at 231 K (Figure 7d−f).

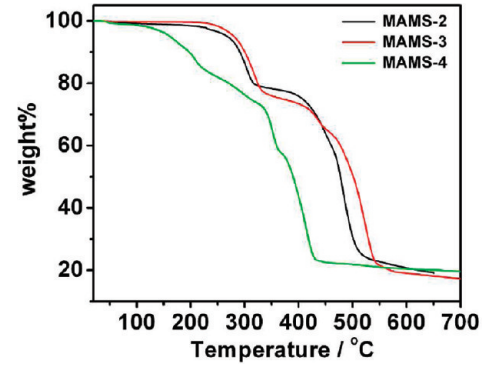

Figure 6. TGA plots of MAMSs.

Gas adsorption studies on activated MAMS-3 and activated MAM-4 reveal almost the same phenomena as discovered in MAMS-2 (see Supporting Information). The temperature-induced molecular-sieving effects of the three MAMSs are very similar to that of MAMS-1. However, unlike MAMS-1 where a significant amount of isobutane can enter the hydrophilic channels (~5.1 Å) and then enter the gas storage space at room temperature,[9] the relative smaller sizes of the channels of the three new MAMSs (~4.9 Å) preclude the entrance of isobutane (kinetic diameter 5.0 Å)[18] leading to very limited uptake. A drawing of temperature versus size of the molecule allowed to enter the gate is given in Figure 8. The gate opening, D, and temperature, T, can be related by a linear equation, $D = 0.0073T + 2.83$, with a correlation coefficient of 0.996 (Figure 8). This is very close to the linear equation found in MAMS-1, $D = 0.0076T + 2.76$. The equation can be used to predict if a gas molecule will be allowed to enter the gate at a certain temperature. It can also be used to find the best temperature for the separation of a mixture. The opening of the gates at 77 K is extrapolated to be 3.4 Å, consistent with the experimental observation that all gas molecules except hydrogen are rejected by the new MAMSs.

Proposed Mechanism Studies. The mechanistic details of these unprecedented temperature-controlled gas-selective adsorption phenomena can be deduced from the crystal structures and adsorption data of the new MAMSs.

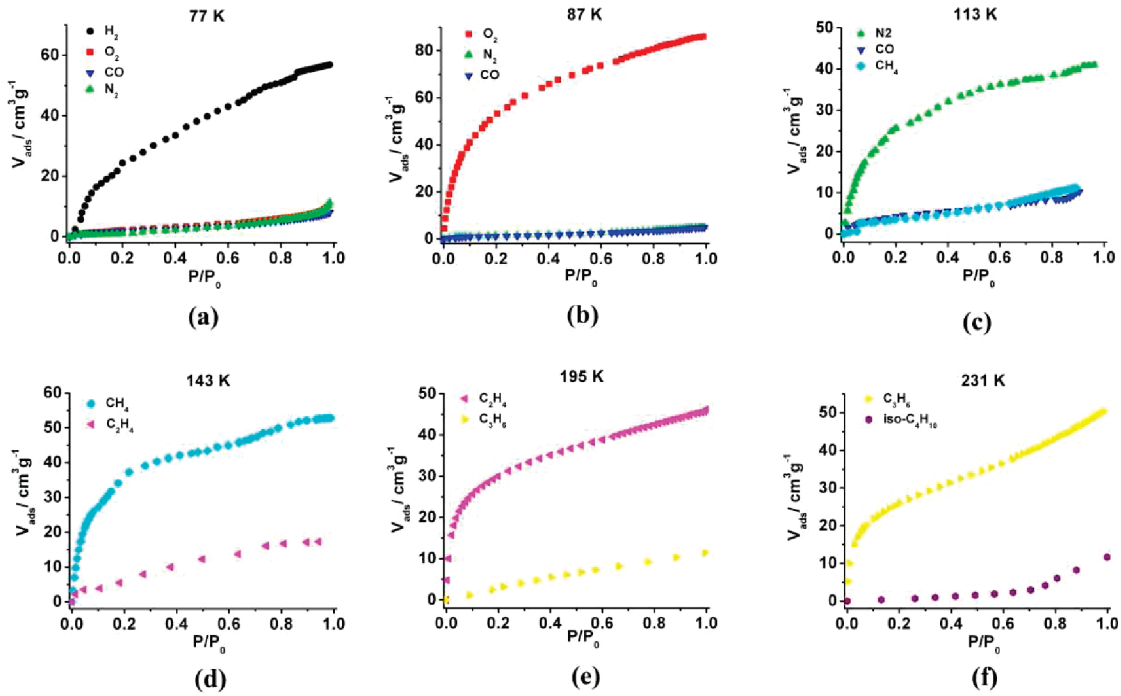

Figure 7. Gas adsorption isotherms of MAMS-2 at six different temperatures (note: P_0 represents a relative standard as specified in the Experimental Section).

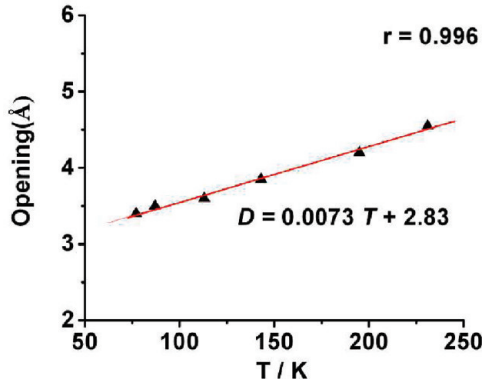

Figure 8. Temperature and gate-opening relationship of MAMS-2. ▲, estimated values based on experimental data; —, linear fit.

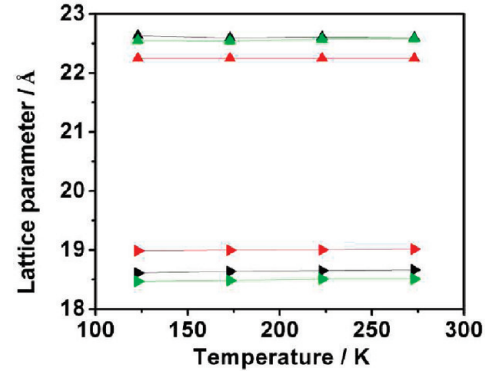

Figure 9. Crystal lattice parameters of MAMSs at different temperatures: sideways arrows represent *a* or *b* axis; upright arrows represent *c* axis; MAMS-2 (black); MAMS-3 (red); MAMS-4 (green).

These temperature-dependent molecular-gating effects do not arise from simple thermal expansion of the framework. As shown in Figure 9, the unit cell parameters of the three new MAMSs remain almost constant while the temperature changes from 113 to 273 K. This assessment is also supported by the temperature independence of powder X-ray diffraction (PXRD). Although MAMS-2 lose crystallinity after activation,[19] the PXRD patterns of activated MAMS-3 and MAMS-4 reveal their framework integrities and no peak shifts have been observed when temperature changes (Figure S15, 16).

The hydrophobic cages are not accessible when the hydrophilic channels are closed, which not only can be inferred from the crystal structure, but is also consistent with gas adsorption data. An inactivated sample had very low uptake of H_2 at 77 K (Figure S1, 3, 9). A partially activated sample was inactive for gas uptake. The DMF (or DMA) guests and bound aqua ligands must be removed completely for MAMSs to be active for gas adsorption.

The hydrophilic channels alone are not responsible for the gas uptake. In fact, they account for only a very small part of the adsorption. As the gas adsorption data at 77 K suggests, only H_2 can enter the hydrophobic gas storage space, showing a significant uptake. At 77 K, other gas molecules stay in the hydrophilic channels and the uptake of these gases is very low, as shown by adsorption studies.

Gas molecules must go through the hydrophilic channel to access the hydrophobic cages. As previously mentioned, activation of the hydrophilic channels is a prerequisite for gas adsorption on MAMSs. Further evidence for the hydrophilic channels being the only passage to the main gas storage space is provided by the observation that when the kinetic diameter of the gas molecule (for example, isobutane, 5.0 Å, and SF_6, 5.5 Å) exceeded the size of the hydrophilic channels (~4.8−4.9 Å considering van der Waals radii), no meaningful uptake was observed in an adsorption study (Figure S2, 8, 14) even at room temperature. The upper limit of the channel is also consistent with an adsorption study on

(19) Eddaoudi, M.; Kim, J.; Rosi, N.; Vodak, D.; Wachter, J.; O'Keeffe, M.; Yaghi, O. M. *Science* **2002**, *295*, 469.

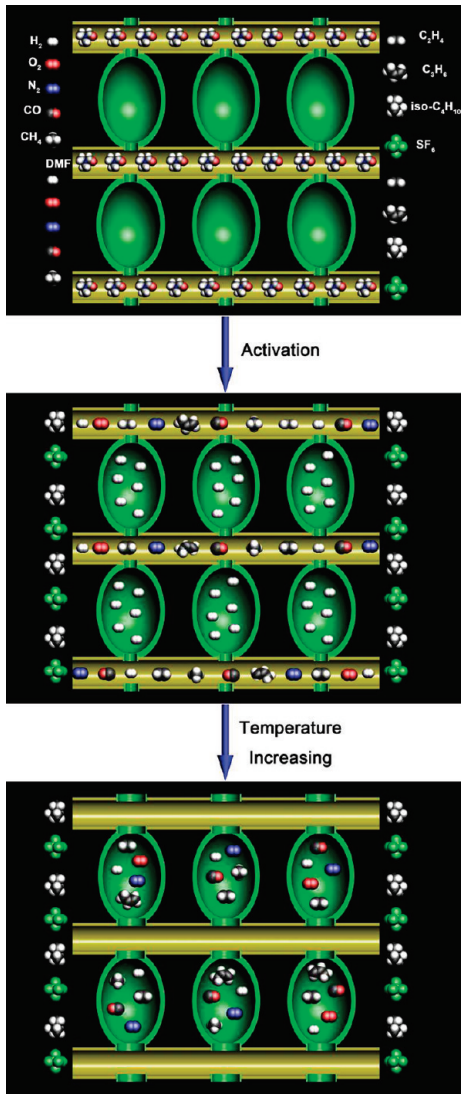

Figure 10. Schematic representation of the mechanism of the temperature-dependent gating effects in MAMSs.

propylene (4.5 Å), which is allowed to enter MAMS-2 at 231 K (Figure 7).

Through the interface between the hydrophobic and hydrophilic channels, gas molecules enter the hydrophobic gas storage cages, which account for the majority of gas uptake. The interface is controlled by a *tert*-butyl group of a BBPDC ligand which inserts in each vertical slit of the cage acting as a gate. The opening of this gate is controlled by thermal motion. When temperature is raised, the van der Waals interaction among the *tert*-butyl groups is reduced, leading to wider gate-opening (Figure 10). As shown in Figure 8, the gate opening, D, and temperature, T, have a linear relationship, $D = 0.0073T + 2.83$, with a correlation coefficient of 0.996 (Figure 8) for the three new MAMSs, implying that the choice of metal is irrelevant to the mesh adjustment. This is very close to the linear equation found in MAMS-1, $D = 0.0076T + 2.76$. This means that in the linear relationship between mesh size and temperature, $D = D_0 + \alpha T$ (D, mesh size at temperature T K; D_0, mesh size at 0 K; and α, constant), D_0 and α are dominated by the *tert*-butyl group. Changing the *tert*-butyl group to other functional groups such as a methyl or isopropyl group can lead to different values for D_0 and α.

Conclusions

In summary, by designing a new amphiphilic ligand, BBPDC, and placing it in solvothermal reactions with $M(NO_3)_2$ (M = Zn, Co, Cu), three new graphitic MOF structures, MAMS-2, MAMS-3, and MAMS-4, generated by the packing of sandwiched layers through van der Waals interaction, were obtained. In each layer, the hydrophilic dimetal paddlewheel cluster layer is sandwiched by two hydrophobic BBPDC layers; every three dimetal paddlewheel clusters are connected to form triangular hydrophilic holes, and every six triangular hydrophilic holes are enclosed to form a hydrophobic cage which serves as the main space for gas storage. Packing of the sandwiched layers generates one-dimensional triangular hydrophilic channels, every six of which surround the hydrophobic cages, which are not accessible without activation. Gas molecules enter the hydrophobic gas storage cages through the hydrophilic channels, and gates in the hydrophobic/hydrophilic interface. The gates are formed by the BBPDC groups inserted in the vertical slits of the hydrophobic cages via van der Waals interaction, which is readily weakened by thermal motion. As temperature increases, the gates of the new MAMSs open linearly, giving rise to molecular sieves with adjustable meshs that can separate any two gases with kinetic diameters in the range of 2.9−4.6 Å, corresponding to the size limits of most commercially relevant gases. There exists a linear relationship between mesh size and temperature, $D = D_0 + \alpha T$ (D, mesh size at temperature T K; D_0, mesh size at 0 K; and α, constant), D_0 and α are only related to the *tert*-butyl group and are not affected by the choice of metal. Changing the *tert*-butyl group to other functional groups such as methyl group or isopropyl group is expected to lead to different values for D_0 and α.

Acknowledgment. This work was supported by the U.S. Department of Energy (DE-FC36-07GO17033) and the U.S. National Science Foundation (CHE-0449634). H.-C.Z. acknowledges the Research Corporation for a Cottrell Scholar Award, and Air Products for a Faculty Excellence Award.

Supporting Information Available: Crystallographic information files (CIFs) of MAMS-2, MAMS-3, MAMS-4, gas adsorption isotherm graphics, and PXRD patterns. This material is available free of charge via the Internet at http://pubs.acs.org.

JA808896F